ECCOMAS Thematic Conference on Multibody Dynamics
July 24 - 28, 2023, Lisbon, Portugal

NMPC-based Control of Overdetermined Systems by the Example of Magnet Control of the Transrapid

Arnim Kargl[1], **Patrick Schmid**[1], **Florian Dignath**[2], **Peter Eberhard**[1]

[1] Institute of Engineering and Computational Mechanics
University of Stuttgart
Pfaffenwaldring 9, 70569 Stuttgart, Germany
[arnim.kargl, patrick.schmid, peter.eberhard]@itm.uni-stuttgart.de

[2] thyssenkrupp Transrapid GmbH
Moosacher Str. 58, 80809 Munich, Germany
florian.dignath@thyssenkrupp.com

ABSTRACT

One common challenge in control design is handling overdetermined systems, i.e., systems with more control inputs than degrees of freedom. The example studied throughout this contribution is the so-called bow magnet of the magnetic levitation (Maglev) vehicle Transrapid. The bow levitation magnets placed at the vehicle's front and rear represent mechatronic systems with two mechanical degrees of freedom, while having three actuator inputs, due to their increased length compared to the standard levitation magnets. Model predictive control (MPC) as a model-based control strategy is already successfully implemented for standard levitation magnets contributing to the levitation system. Therefore, this work studies the application of nonlinear MPC methods at the bow magnet as an example of an overdetermined system. A classical implementation using one individual control algorithm per control input of the magnet is compared to a newly developed control scheme of one centralized controller for the whole magnet. Advantages, as well as disadvantages of both schemes are discussed.

Keywords: High-speed Maglev Vehicle, Model Predictive Control, Overdetermined System, Mechatronics.

1 INTRODUCTION

The first step in model-based control design is acquiring simulation models of the system's underlying dynamics. Thereby, different levels of detail describing this dynamics are taken into account. While control design usually is done with simplified surrogate models, the resulting algorithms are then analyzed in a highly detailed model of the complete system. Particularly for model predictive control, suitable descriptions of the system dynamics have to be found to carry out the prediction of the system's behavior within the control algorithm.

In case of the Maglev vehicle Transrapid, see Figure 1, the principle of the magnetic wheel as an autonomous functional unit is realized. Thereby, the vehicle's levitation system consists of levitation chassis and levitation magnets forming a decoupling structure. This results in each half of a standard levitation magnet only being weakly coupled to its adjoint levitation magnets, allowing for isolated control. As derived in [1], the Lyapunov stability of the complete vehicle follows from the stability of the individual, weakly coupled subsystems, greatly simplifying the control design task. Therefore, in the case for standard levitation magnets [2], a control subsystem can be mapped by a magnetically levitated mass point with one degree of freedom as shown in Figure 2(a). In contrast, the assumption of weak coupling does not hold for the bow levitation magnets at the front and rear end of the vehicle being an overdetermined system. Therefore, an alternative control subsystem for the bow levitation magnets is studied in this contribution taking the whole magnet body with two degrees of freedom into account as shown in Figure 3.

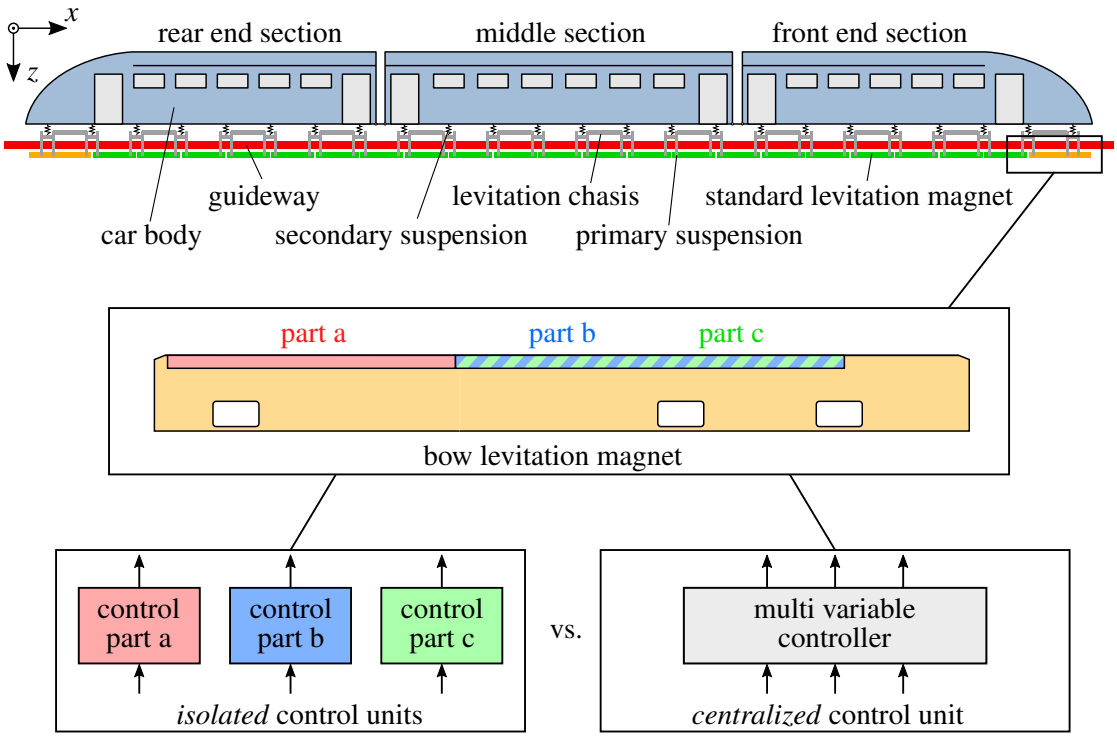

Figure 1. Schematic illustration of the Maglev vehicle Transrapid with focus on control of the bow levitation magnets. Figures adapted from [3] (vehicle model) and [4] (bow magnet).

Method and Contribution. The control of the bow levitation magnet for both subsystem variants is realized by nonlinear model predictive control. While a control scheme from [2] is adapted for isolated control of the bow magnet circuits, a new centralized control algorithm is developed for the complete bow levitation magnet, see Figure 1. Advantages as well as disadvantages of this newly developed control scheme are discussed with aid of simulations of the surrogate control subsystem model as well as a highly detailed, large-scale vehicle model.

A detailed description of both control subsystems and a brief introduction to the detailed vehicle model for analysis purposes, is given in Section 2. The design and implementation of the NMPC algorithms is covered in Section 3. Finally, results for both control strategies, as well as advantages and disadvantages in different scenarios, are discussed in Section 4. Section 5 concludes the contribution.

2 MODELING

The simulation model of each control subsystem, briefly described above, has to map the relevant dynamics corresponding to the real mechatronic system. In particular, such a model should map the mechanics of the subsystem and the electrodynamics of the involved electromagnet with suitable detail. The model interface in terms of inputs and outputs is motivated by the actuation and available measurements at the real system.

2.1 Magnetically Levitated Mass for Control Design

For the implementation of one individual control algorithm per electric circuit of a levitation magnet, the surrogate control subsystem is given by a magnetically levitated mass with one degree of freedom z, see Figure 2(a). Its mechanical representation in terms of a second order ordinary differential equation (ODE) directly follows from Newton's second law

$$m\ddot{z} = mg + F_{\mathrm{L}} - F_{\mathrm{mag}}(s, I), \tag{1}$$

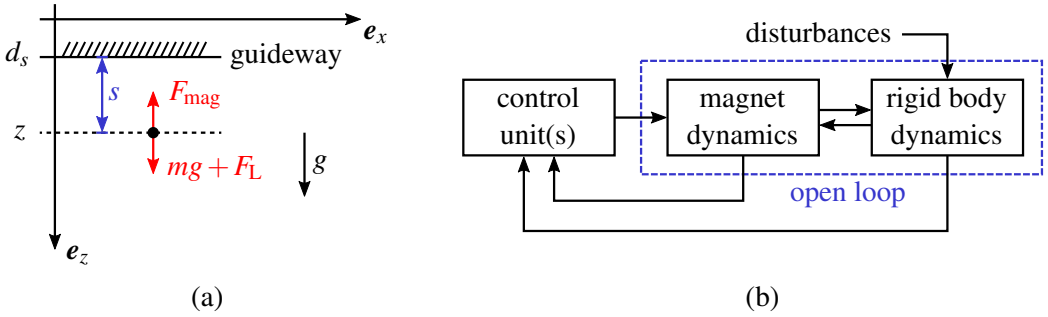

Figure 2. Kinematics for the levitated mass model (a) and general structure of closed-loop dynamics coupled in Matlab / Simulink (b).

where m denotes the surrogate mass, g the gravitational constant, F_{L} a constant force approximating the load of the vehicle onto the magnet and F_{mag} the magnetic force. The latter is a function of the air gap s between magnet and guideway and the electric current I within the electric circuit of the electromagnet. The measured air gap $s = z - d_s$ results from the vertical position of the mass and the guideway disturbance d_s acting on the model.

Modeling the dynamics of the electromagnet itself follows the approach described in [5] resulting in one first order nonlinear ODE in the electric current I for the electric circuit of the magnet part

$$\dot{I} = -\alpha(s,\dot{s},I)\,I + \beta(s,I)\,U. \tag{2}$$

Its nonlinearity is characterized by the functions α and β depending on the state I and the inputs s and $\dot{s}$ given by the mechanical model. Input to the electric circuit is the voltage U applied by the controller. The simplified structure of the magnet dynamics make it suitable for control design in contrast to, e.g., a formulation as differential algebraic equation in the magnetic flux, also described in [5]. Although simplified, this model, however, still covers all relevant physical effects such as magnetic saturation, leakage fluxes, and eddy currents. For later simulation of the closed loop the individual components are coupled in Matlab / Simulink as shown in Figure 2(b). This modular design allows for quickly testing multiple model variants, e.g., different control algorithms.

For control design, however, the dynamics of the coupled components, i.e., Equations (1) and (2), are needed in state-space representation with the equilibrium point being at the origin. First, the system state $\boldsymbol{x} := [s,\dot{z},I]^{\mathrm{T}}$ is defined. Second, the equilibrium point $(\boldsymbol{x}_0,U_0) = \left([s_0,0,I_0]^{\mathrm{T}},U_0\right)$ is shifted to the origin, leading to new coordinates $\Delta x := x - x_0$ and $\Delta U := U - U_0$. With those, the dynamics of the coupled system consisting of mechanics and magnet model can be described by

$$\Delta\dot{\boldsymbol{x}} = \begin{bmatrix} \dot{s} \\ \ddot{z} \\ \dot{I} \end{bmatrix} = \begin{bmatrix} \dot{z} \\ g + \frac{F_{\mathrm{L}} - F_{\mathrm{mag}}(s_0+\Delta s,\, I_0+\Delta I)}{m} \\ -\alpha(s,\dot{z},I)\,I + \beta(s,I)\,(U_0+\Delta U) \end{bmatrix} =: \boldsymbol{f}(\Delta\boldsymbol{x},\,\Delta U). \tag{3}$$

Note that it formally holds that $s = z - d_s$ and further $\dot{s} = \dot{z} - \dot{d}_s$. However, for control design the disturbance d_s is unknown and therefore assumed to be zero, i.e., $d_s \equiv 0$. Moreover, the choice of state variables is motivated by the available measurements, namely the air gap s, the vertical acceleration $\ddot{z}$, and the electric current I.

2.2 Bow Magnet Model for Control Design

The control subsystem formed by the magnetically levitated mass is well suited for standard levitation magnets. However, for the overdetermined bow levitation magnet the assumption of weak coupling between the magnet parts does no longer hold. Here, three independent magnet forces

resulting from three electric circuits act on one rigid body with two degrees of freedom. Therefore, a larger control subsystem has to be taken into account. In this contribution the whole bow levitation magnet serves as surrogate model for control design as shown in Figure 3. The particular structure of the magnet is taken from [4]. On the mechanical side the model consists of the magnet body with two degrees of freedom z and φ collected in the vector of generalized coordinates $\boldsymbol{y} := [z, \varphi]^{\mathrm{T}}$. Three concentrated magnet forces $F_{\mathrm{mag},i}$, $i \in \{a,b,c\}$ lift the magnet body, while static forces $F_{\mathrm{L},j}$, $j \in \{1,2,3\}$ at its support points approximate the load of the vehicle resting on the magnet. The equations of motion of the mechanical system are derived in a symbolic manner with the multibody systems toolbox Neweul-M^2 [6] and can formally be expressed as

$$\boldsymbol{M}(\boldsymbol{y})\ddot{\boldsymbol{y}} = \boldsymbol{q}(\boldsymbol{y}, \dot{\boldsymbol{y}}, \boldsymbol{F}_{\mathrm{mag}}). \tag{4}$$

Thereby $\boldsymbol{M}$ represents the positive definite mass matrix and $\boldsymbol{q}$ is the vector of generalized applied forces with the system input $\boldsymbol{F}_{\mathrm{mag}} := [F_{\mathrm{mag},a}, F_{\mathrm{mag},b}, F_{\mathrm{mag},c}]^{\mathrm{T}}$. The interaction with the guideway is implemented in a unilateral fashion, such that reference points on the guideway, e.g., for gap measurement, are movable in vertical direction to apply pre-computed disturbance profiles over time. On the electrical side the poles of each magnet part are interconnected and form one electric circuit per part. For magnet parts b and c, the magnet poles are wired in a nested way motivated by the distribution of the resulting concentrated magnet forces. Although this nested wiring leads to stronger coupling of neighboring circuits via the magnetic flux, each circuit can still be modeled in an isolated fashion, as the coupling is less than 5 % as measured by the current flow. Therefore, the magnet dynamics are modeled analogously to Section 2.1 by one decoupled ODE per electric circuit

$$\dot{I}_i = -\alpha_i(s_i, \dot{s}_i, I_i)\, I_i + \beta_i(s_i, I_i)\, U_i, \quad i \in \{a,b,c\} \tag{5}$$

with the individual output $F_{\mathrm{mag},i} = F_{\mathrm{mag},i}(s_i, I_i)$ as a function of the air gap s_i and the electric current I_i. For further use, the inputs U_i are collected in $\boldsymbol{U} := [U_a, U_b, U_c]^{\mathrm{T}}$, and the vector of the electric currents is defined as $\boldsymbol{I} := [I_a, I_b, I_c]^{\mathrm{T}}$. With that, the magnet dynamics of the complete system can be expressed as

$$\dot{\boldsymbol{I}} = -\boldsymbol{A}(\boldsymbol{s}, \dot{\boldsymbol{s}}, \boldsymbol{I})\, \boldsymbol{I} + \boldsymbol{B}(\boldsymbol{s}, \boldsymbol{I})\, \boldsymbol{U} \tag{6}$$

with diagonal functionals $\boldsymbol{A} := \mathrm{diag}(\alpha_a, \alpha_b, \alpha_c)$ and $\boldsymbol{B} := \mathrm{diag}(\beta_a, \beta_b, \beta_c)$. Again, for control design, the coupled system needs to be available in state-space form. Therefore, the state $\boldsymbol{x} := [\boldsymbol{y}^{\mathrm{T}}, \dot{\boldsymbol{y}}^{\mathrm{T}}, \boldsymbol{I}^{\mathrm{T}}]^{\mathrm{T}}$ is introduced. Analogously to Section 2.1, the equilibrium $(\boldsymbol{x}_0, \boldsymbol{U}_0)$ is translated to the origin via $\Delta\boldsymbol{x} := \boldsymbol{x} - \boldsymbol{x}_0$ and $\Delta\boldsymbol{U} := \boldsymbol{U} - \boldsymbol{U}_0$ leading to the ODE

$$\Delta\dot{\boldsymbol{x}} = \begin{bmatrix} \dot{\boldsymbol{y}} \\ \ddot{\boldsymbol{y}} \\ \dot{\boldsymbol{I}} \end{bmatrix} = \begin{bmatrix} \dot{\boldsymbol{y}} \\ \boldsymbol{M}^{-1}(\boldsymbol{y})\, \boldsymbol{q}\left(\boldsymbol{y}, \dot{\boldsymbol{y}}, \boldsymbol{F}_{\mathrm{mag}}(\boldsymbol{s}, \boldsymbol{I})\right) \\ -\boldsymbol{A}(\boldsymbol{s}, \dot{\boldsymbol{s}}, \boldsymbol{I})\, \boldsymbol{I} + \boldsymbol{B}(\boldsymbol{s}, \boldsymbol{I})\, \Delta\boldsymbol{U} \end{bmatrix} =: \boldsymbol{f}(\Delta\boldsymbol{x}, \Delta\boldsymbol{U}). \tag{7}$$

Since the air gaps $\boldsymbol{s} := [s_a, s_b, s_c]^{\mathrm{T}}$ and their time derivatives are not part of the system's state, they have to be computed by output equations $\boldsymbol{s} = \boldsymbol{s}(\boldsymbol{y}) = \boldsymbol{s}(\boldsymbol{x}_0 + \Delta\boldsymbol{x}) = \boldsymbol{s}(\Delta\boldsymbol{x})$ and $\dot{\boldsymbol{s}} = \dot{\boldsymbol{s}}(\Delta\boldsymbol{x})$.

2.3 Large-scale Vehicle Model for Analysis

For analysis of the control algorithms developed next, a highly detailed two-dimensional model of the Transrapid is available, see Figure 1. The model is introduced in [3] and consists of three vehicle sections traveling over a guideway of infinite length formed by elastic Euler-Bernoulli beams. Being a two-dimensional longitudinal cut through the vehicle, it maps heave and pitch motions of all involved rigid components such as car bodies, levitation chassis, and levitation magnets. The equations of motion are derived with the multibody systems toolbox Neweul-M^2 and parameterized according to the latest Transrapid vehicle TR09. Each magnet's electric circuit is equipped with the corresponding electrodynamics equation of form (2) and is controlled by an individual control input. The coupling of the vehicle components again adopts the structure shown in Figure 2(b).

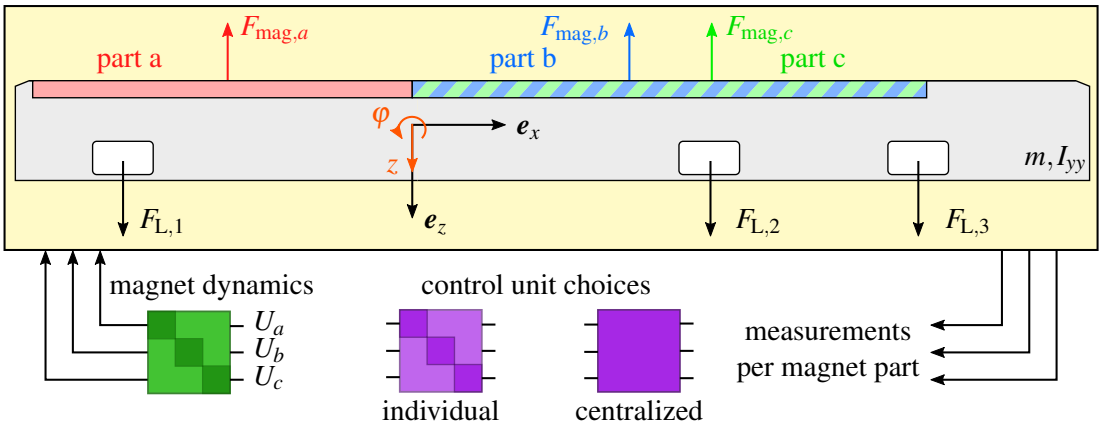

Figure 3. Control subsystem for the bow levitation magnet consisting of rigid body dynamics, magnet model. The closed-loop is formed with either three individually acting control units or one centralized control unit.

3 CONTROL DESIGN

This section deals with designing two model predictive control strategies for the bow levitation magnet. First, the design of one centralized MPC algorithm for the control subsystem introduced in Section 2.2 is described. Second, one individual MPC algorithm per electric circuit, equipped with the prediction model from Section 2.1, is designed following a particular offset-free approach proposed in [2].

3.1 Equilibrium Points

Prior to the specific design of control algorithms, a brief discussion about finding equilibrium points for the overdetermined system is needed. In general, the desired nominal air gap between magnet and guideway together with the equations of motion from the system's mechanics determines the magnet forces in equilibrium. This assignment, however, is not unique since three independent magnet forces act on the magnet body with two degrees of freedom. One approach for given generalized coordinates $\boldsymbol{y}_0$ is to use the additional degree of freedom in design by solving an optimization problem of the form,

$$\underset{\boldsymbol{F}_{\mathrm{mag},0}}{\text{minimize}} \quad \boldsymbol{F}_{\mathrm{mag},0}^{\mathrm{T}} \boldsymbol{Q}_0 \boldsymbol{F}_{\mathrm{mag},0} \tag{8a}$$

$$\text{subject to} \quad \boldsymbol{q}(\boldsymbol{y}_0, \boldsymbol{0}, \boldsymbol{F}_{\mathrm{mag},0}) = \boldsymbol{0}. \tag{8b}$$

The constraint in Equation (8b) enforces the mechanical equilibrium according to Equation (4), while the cost function in (8a) can be used to influence the force distribution. In case of the bow levitation magnet, quadratic costs with positive definite weighting matrix $\boldsymbol{Q}_0$ are applied. Knowledge of the nominal magnet force per magnet part then allows computing the nominal electric current and voltage via the magnet model.

3.2 Centralized MPC Design

In contrast to classical control schemes, e.g., a linear quadratic regulator, where a control law is computed offline, the control law in model predictive control is computed online. Therefore, at a given point in time an open-loop optimal control problem (OCP) is solved predicting the system's behavior over a certain time interval, namely the prediction horizon. Solution to the OCP is an optimal input trajectory to the system. However, only the first part of this input trajectory is applied to the real plant up to the next sampling point, when the process is repeated. This leads to the prediction horizon moving forward in time, which is why MPC is often called receding

horizon control. One major advantage in comparison to classical control algorithms is the possibility to directly handle constraints on the system dynamics and inputs within the OCP. A general introduction to nonlinear model predictive can be found in [7].

With these prerequisites, the formulation of an MPC scheme for the control subsystem (7) of the whole bow levitation magnet requires only one further topic to mention, namely the use of an offset-free scheme. The latter ensures offset-free tracking in presence of quasi-static disturbances, such as different load of the vehicle. Therefore, the system dynamics (7) is augmented by an integral state $\boldsymbol{w_y}$ yielding

$$\Delta\dot{\boldsymbol{x}}_{\text{aug}} = \begin{bmatrix} \Delta\dot{\boldsymbol{x}} \\ \dot{\boldsymbol{w}}_{\boldsymbol{y}} \end{bmatrix} = \begin{bmatrix} \boldsymbol{f}(\Delta\boldsymbol{x}, \Delta\boldsymbol{U}) \\ \boldsymbol{y} - \boldsymbol{y}_0 \end{bmatrix} =: \boldsymbol{f}_{\text{aug}}(\Delta\boldsymbol{x}_{\text{aug}}, \Delta\boldsymbol{U}). \tag{9}$$

More involved offset-free strategies are available and can, e.g., be found in [2]. In sum, the augmented open-loop dynamics consists of nine states and three input variables. The resulting nonlinear MPC scheme at time t can finally be formulated in continuous time and reads as

$$\begin{aligned}
\underset{\Delta\boldsymbol{U}(\cdot;\,t)}{\text{minimize}} \quad & \int_t^{t+T} \Delta\boldsymbol{x}_{\text{aug}}^{\text{T}}(\tau;\,t)\,\boldsymbol{Q}\,\Delta\boldsymbol{x}_{\text{aug}}(\tau;\,t) + \Delta\boldsymbol{U}^{\text{T}}(\tau;\,t)\,\boldsymbol{R}\,\Delta\boldsymbol{U}(\tau;\,t)\,\mathrm{d}\tau && \text{(10a)} \\
\text{subject to} \quad & \Delta\dot{\boldsymbol{x}}_{\text{aug}}(\tau;\,t) = \boldsymbol{f}_{\text{aug}}\left(\Delta\boldsymbol{x}_{\text{aug}}(\tau;\,t), \Delta\boldsymbol{U}(\tau;\,t)\right), \quad \forall\tau \in (t,\,t+T) && \text{(10b)} \\
& \boldsymbol{x}_{\text{aug}}(t;\,t) = \boldsymbol{x}_{\text{aug}}(t), && \text{(10c)} \\
& U_{\min} \leq U_{0,i} + \Delta U_i(\tau;\,t) \leq U_{\max}, \quad \forall\tau \in [t,\,t+T],\; i \in \{a,b,c\}\,. && \text{(10d)}
\end{aligned}$$

Therein, $\Delta\boldsymbol{U}(\cdot;\,t)$ denotes the control input to system (9) predicted at time t. Equation (10b) ensures the predicted state $\boldsymbol{x}_{\text{aug}}(\cdot;\,t)$ to comply with the system dynamics, initialized by assuming a full state measurement in Equation (10c). With Equation (10d), actuator constraints of the real-world system are satisfied. The cost function (10a) is chosen to be convex quadratic with $\boldsymbol{Q} \geq 0$ and $\boldsymbol{R} > 0$. Note that path and terminal constraints as well as the proof for theoretical stability are omitted due to practical reasons.

3.3 Individual MPC Design

For comparison, one individual model predictive controller per control input of the bow levitation magnet is designed, as done in [2]. The procedure is analog to Section 3.2 using the control subsystem's dynamics (3). Again, the dynamics is augmented by an integral state allowing for offset-free stabilization of the origin

$$\Delta\dot{\boldsymbol{x}}_{\text{aug}} = \begin{bmatrix} \Delta\dot{\boldsymbol{x}} \\ \dot{w}_s \end{bmatrix} = \begin{bmatrix} \boldsymbol{f}(\Delta\boldsymbol{x}, \Delta U) \\ s - s_0 \end{bmatrix} =: \boldsymbol{f}_{\text{aug}}(\Delta\boldsymbol{x}_{\text{aug}}, \Delta U). \tag{11}$$

The optimal control problem can be stated equivalently to (10) with adapted dimensions for $\boldsymbol{Q}$ and $\boldsymbol{R}$, and with just four states and one input, respectively.

3.4 MPC Implementation

The MPC schemes developed in Sections 3.3 and 3.2 are implemented with GRAMPC [8]. The tool implements an implicit MPC algorithm with indirect discretization in form of a gradient projection method, suitable for fast MPC and even deployable to embedded systems. For technical details the interested reader is referred to [8]. The system dynamics, cost function, and constraint functions are set up with CasADi [9], allowing the computation of gradients needed by GRAMPC via automatic differentiation. Furthermore, CasADi's built-in export capabilities are used to convert the derived Matlab functions to C. The resulting algorithm can be run as a Simulink S-function or with only little further effort on a microcontroller in an existing Processor-in-the-Loop setup [10].

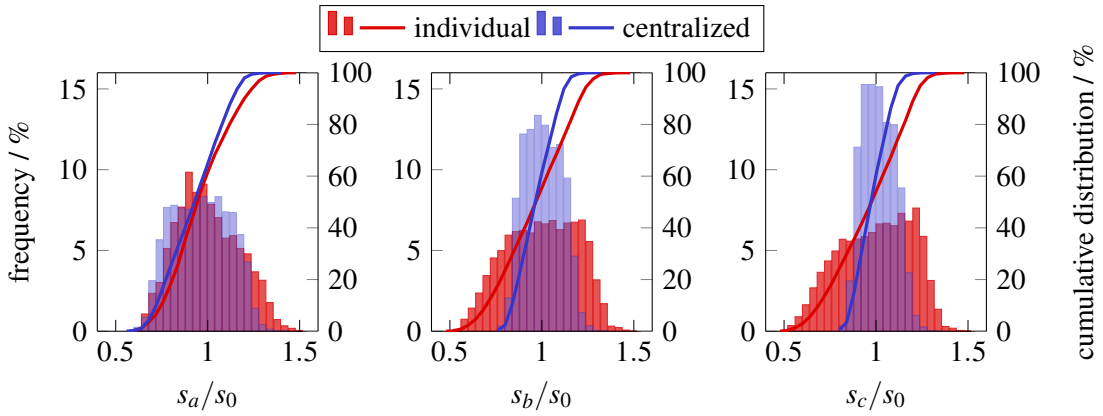

Figure 4. Air gap histograms for simulation of the levitated bow magnet model in nominal operation at 400 km/h for both control schemes.

4 RESULTS

In the following, the newly developed MPC scheme from Section 3.2 is compared to the approach with individual MPC controllers, adapted in Section 3.3, for various simulation scenarios. First, the behavior of both algorithms is investigated with the model of the single levitated bow magnet from Section 2.2. The simulation is carried out at a speed of 400 km/h influenced by a statistical model of the guideway disturbances introduced in [11]. As a measure of performance, the air gap normalized by the desired air gap s_0 is plotted in histograms in Figure 4. One observes the centralized MPC approach being able to track the desired air gap better than the individual controllers. Especially at magnet parts b and c, differences in control performance are visible. Some effort on tuning the individual control algorithms to match the performance of the centralized MPC was made, however, without any remarkable improvements.

The main advantage of the centralized control approach for the overdetermined system can be seen in a scenario with static measurement error, e.g., due to production tolerance. Therefore, the air gap s_c is manipulated at $t = 2\,s$ by adding 20 % of the nominal air gap to the measure, an arguably large offset for demonstration reasons. The simulation is done without the high frequent guideway disturbance to see the effect more clearly. Figures 5 and 6 show the resulting current and resulting air gaps at the plant, respectively, for both control strategies. Both control algorithms immediately try to counter the observed step in the gap measurement. However, due to the magnet body being modeled rigid, the nominal air gap as seen by the controller cannot simultaneously be reached at all three magnet parts anymore. For the isolated controllers this leads to contrary behavior, visible as drift in the current signals, finally reaching instability at $t \approx 10\,\mathrm{s}$. On the other hand, the single, centralized control algorithm utilizes its information about the whole magnet's state to find an optimal trade-off in terms of its cost function. After a transition phase, this results in slightly tilting the magnet body.

Finally, the performance of the two control algorithms is evaluated in the large-scale vehicle model introduced in Section 2.3. With the model, a highly realistic environment for analyzing and evaluating different control approaches is given. For this study, both introduced control algorithms are implemented at the bow magnet, while the remaining standard levitation magnets are controlled by further individual MPC controllers presented in [2]. Control performance is analyzed at the rear bow magnet, being the most challenging magnet to control as pointed out in [3]. Figure 7 shows the resulting air gaps for each bow magnet part obtained during simulation of the vehicle model at 300 km/h on the elastic guideway. Similar to the previously shown results at the isolated bow magnet model, compare Figure 4, the centralized control algorithm achieves better control performance by means of a smaller deviation from the desired air gap s_0.

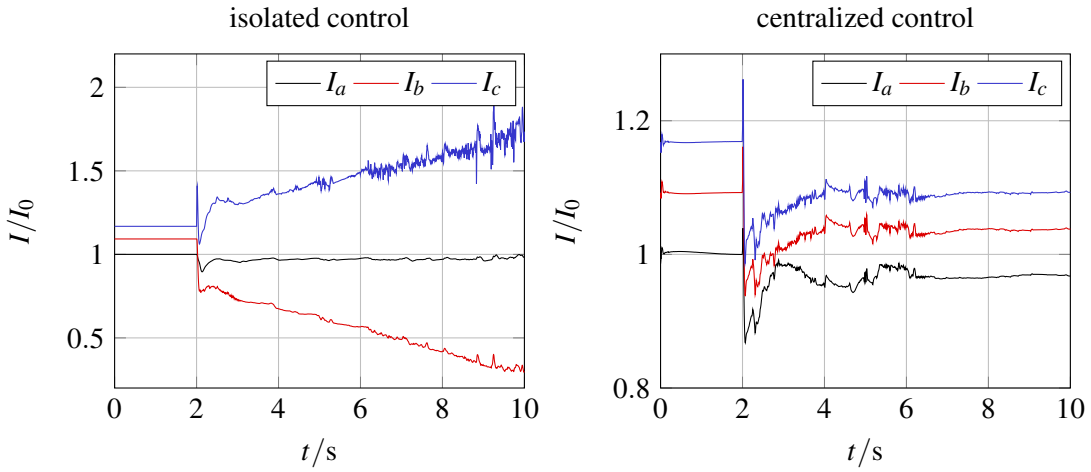

Figure 5. Current signals of the bow levitation magnet under static measurement error.

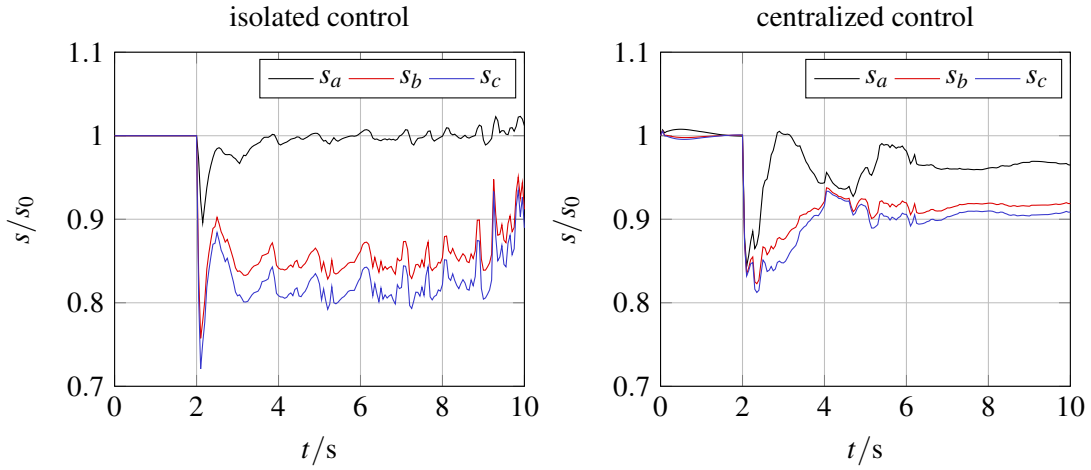

Figure 6. Mechanical air gaps at the magnet when a measurement error of 2 mm is introduced at $t = 2\,\mathrm{s}$ into the control system.

With these results the centralized control algorithm for the whole magnet is shown beneficial compared to the classical approach with three individually acting controllers. However, there are also some disadvantages to mention, especially regarding the implementation at the real system. The control subsystem for the whole bow magnet, formulated in Equation (9), leads to overall nine states as well as three inputs with individual input constraints to handle by the optimal control problem (10). Despite recent developments in numerical algorithms to solve problem (10), a real-time capable implementation with the increased number of states and inputs is still challenging. On the other hand, for the individual control approach real-time capability can be shown [10]. Furthermore, the discussed algorithm assumes full state measurement which is not available at the real-world system. Additional techniques such as state filtering or observer-based approaches have to be deployed, again, introducing a non-trivial problem due to the system being overdetermined. Finally, concerning failure of a control unit, three individually acting controllers come with an inherent redundancy, which is not the case for the centralized control algorithm.

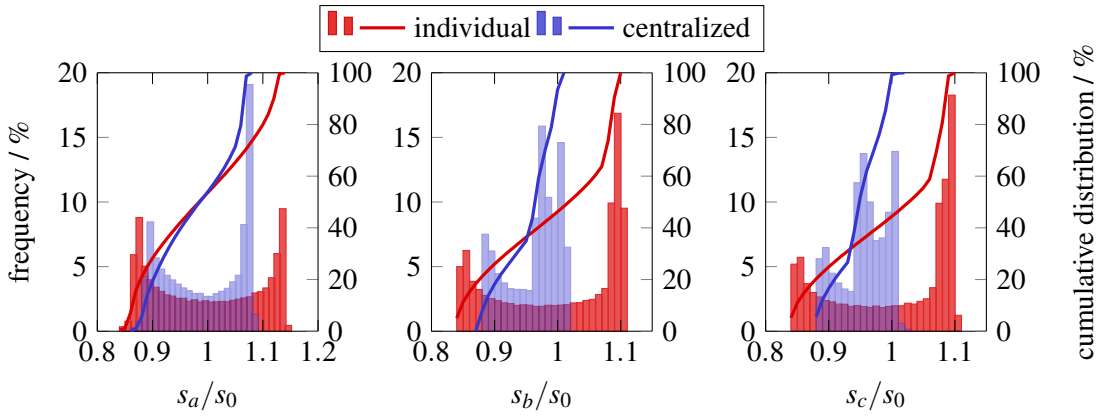

Figure 7. Control performance of both control strategies at the rear bow magnet in the large-scale vehicle model shown in Figure 1.

5 CONCLUSION

In this contribution, nonlinear model predictive control is successfully implemented for an overdetermined system, namely the bow levitation magnet of the Transrapid. Following the approach of the magnetic wheel, three individual MPC controllers acting on the magnet are adapted from [2]. In contrast, a newly developed control algorithm takes the system dynamics of the whole bow magnet into account forming a centralized control approach. The latter is shown beneficial in nominal operation as well as in special scenarios, e.g., in presence of static measurement offsets. For implementation at the real-world system, however, further aspects have to be considered, real-time capability and redundancy of the introduced control strategy being two of them. Especially concerning real-time capability, the deployment of the developed control algorithm to an existing Processor-in-the-Loop setup [10] would give valuable insight. Future work may address these challenges or study the application of alternative control design methods for the system at hand.

REFERENCES

[1] Gottzein, E.: Das Magnetische Rad als autonome Funktionseinheit modularer Trag- und Führsysteme für Magnetbahnen (in German). VDI-Verlag GmbH, Düsseldorf (1984)

[2] Schmid, P., Eberhard, P.: Offset-free Nonlinear Model Predictive Control by the Example of Maglev Vehicles. IFAC-PapersOnLine **54**(6) (July 2021) 83–90 7th IFAC Conference on Nonlinear Model Predictive Control NMPC 2021.

[3] Schneider, G., Schmid, P., Dignath, F., Eberhard, P.: Modeling and Simulation of a High-speed Maglev Vehicle on an Infinite Elastic Guideway. In Kövecses, J., Stépán, G., Zelei, A., eds.: Proceedings of the 10th ECCOMAS Thematic Conference on Multibody Dynamics, Budapest University of Technology and Economics (2021) 420–431

[4] German Federal Railway Authority (EBA): Design Principles High-speed Maglev System (MSB). Technical report (2007). In particular Document no. 57288, p. 30f.

[5] Schmid, P., Schneider, G., Dignath, F., Liang, X., Eberhard, P.: Static and Dynamic Modeling of the Electromagnets of the Maglev Vehicle Transrapid. IEEE Transactions on Magnetics **57**(2) (2021) 1–15

[6] Kurz, T., Eberhard, P., Henninger, C., Schiehlen, W.: From Neweul to Neweul-M^2: Symbolical Equations of Motion for Multibody System Analysis and Synthesis. Multibody System Dynamics **24**(1) (2010) 25–41

[7] Rawlings, J.B., Mayne, D.Q., Diehl, M.: Model Predictive Control: Theory, Computation, and Design. Volume 2. Nob Hill Publishing, Madison, Wisconsin, USA (2017)

[8] Englert, T., Völz, A., Mesmer, F., Rhein, S., Graichen, K.: A Software Framework for Embedded Nonlinear Model Predictive Control using a Gradient-based Augmented Lagrangian Approach (GRAMPC). Optimization and Engineering **20**(3) (2019) 769–809

[9] Andersson, J.A.E., Gillis, J., Horn, G., Rawlings, J.B., Diehl, M.: CasADi – A Software Framework for Nonlinear Optimization and Optimal Control. Mathematical Programming Computation **11**(1) (2019) 1–36

[10] Scheuble, D.: Implementation of MPC Algorithms on a Microcontroller by the Example of Magnet Control of the Transrapid. Master Thesis MSC-318, Institute of Engineering and Computational Mechanics, University of Stuttgart (2021)

[11] Zheng, Q., Dignath, F., Schmid, P., Eberhard, P.: Ride Comfort Transfer Function for the MAGLEV Vehicle Transrapid. In: 4th International Conference on Railway Technology: Research, Development and Maintenance, Barcelona (September 2018). Presentation slides available at http://dx.doi.org/10.18419/opus-11268.